COMBINING NUMERICAL AND EXPERIMENTAL METHODS TO EXPLAIN SHIP-BANK INTERACTIONS

Bedos, Antoine, MARIN, The Netherlands

Gornicz, Tomasz, MARIN, The Netherlands

Tonelli, Roberto, MARIN, The Netherlands

COMBINING NUMERICAL AND EXPERIMENTAL METHODS TO EXPLAIN SHIP-BANK INTERACTIONS

BEDOS, ANTOINE, MARIN, THE NETHERLANDS
GORNICZ, TOMASZ, MARIN, THE NETHERLANDS
TONELLI, ROBERTO, MARIN, THE NETHERLANDS

SUMMARY

Bank effects refer to the suction and repulsion forces a ship experiences when sailing near a bank. Recently, various factors have driven the maritime community to gain a deeper understanding of this phenomenon. In inland waterways, increasing traffic and repeated low-water episodes result in ships operating in increasingly confined environment, leading to stronger interactions with banks and other ships. This paper compares experimental and numerical methods in a straightforward test case involving a representative 135m inland waterway ship sailing along a vertical bank. The study examines the total loads and squat of the ship at various distances to the bank and under-keel clearances, ranging from 300% to 20%. It also verifies several new functionalities in the MARIN in-house CFD package ReFRESCO, which can be used for calculations of complex scenarios involving ships navigating in confined and shallow water.

NOMENCLATURE

δ	Rudder angle (deg)
λ	Linear scale ratio (-)
ρ	Fresh-water density (1,000 kg/m^3)
θ	Pitch angle (deg)
A_C	Cross-sectional area of the waterway (m^2)
A_S	Ship's underwater midship cross-sectional area (m^2)
B	Ship breadth (m)
C_P	Dynamic pressure coefficient (-)
d	Distance between the ship side and the bank (m)
d/B	Non-dimensional distance to bank (-)
F_r	Froude number (-)
F_{rh}	Depth Froude number (-)
F'_X	Ship surge force (-)
F'_Y	Ship sway force (-)
h	Water depth (m)
h/T	Water depth-to-draught ratio (-)
L_{PP}	Ship length between perpendiculars (m)
M'_Z	Ship yaw moment (-)
T	Ship draught at rest (m)
RPM	Propeller revolution rate (1/min)
S	Blockage factor A_S/A_C (-)
V_{cr}	Critical canal speed (km/h or m/s)
V_s	Ship speed (km/h or m/s)
y+	Thickness of the first viscous layer cell (-)

BAW	German Federal Waterways Engineering and Research Institute
CFD	Computational Fluid Dynamics
CFD FS	CFD calculations at full scale
CFD MS	CFD calculations at model scale
EXP	Experiments
MARIN	Maritime Research Institute Netherlands
DST	Development Centre for Ship Technology and Transport Systems
SHINING	Shallow Water Inland Ships Manoeuvring working group
VoF	Volume of Fluid

1 INTRODUCTION

Bank effects (or ship-bank interactions) describe the hydrodynamic interaction between a sailing ship and a nearby boundary of the sailing area, typically a quay in ports or a bank on inland waterways. The restricted space influences the flow and pressure fields around the ship, altering its navigation behaviour compared to a fully unrestricted environment.

Research on bank effects was initiated in the mid-20th century, but regained interest in the last few years following recent events. In 2021, the 20,000 TEU container vessel Ever Given collided with a bank of the Suez Canal and obstructed it for several days, illustrating the race for ever larger ships sailing through very confined channels and locks. In inland waterways, the increasing traffic and repeated low-water episodes result in ships sailing in increasingly confined environment and experiencing stronger interactions with banks. A large share of the research consists in predicting the increase in resistance and squat when sailing near a bank (Lataire et al., 2015, Raven, 2019;), or in deriving reduced-order models to quantify the suction and repulsion forces resulting from the ship-bank interaction (Norrbin, 1985; Delefortrie et al., 2024).

These models aim to be implemented in ship-handling simulators for crew training, design of ports and waterways, accident investigations, and definition of guidelines and regulations. Navigation models must be reliable for comprehensive and complex scenarios, including shallow and confined waterways with dense and potentially dangerous traffic situations. The prediction of ship-bank interactions within these models needs to be accurate enough to result in a realistic behaviour, and fast enough to calculate the hydrodynamic loads in real time. These tools are essential to ensure safe and efficient navigation of vessels in confined environment. As an example, Bedos et al. (2019) investigated the impact of an irregular bank on the sailed trajectory of an inland ship in a river and the risk of collision with a nearby bridge. Mai et al. (2021) assessed the effects of manoeuvring near a bank and in shallow water for an autonomous ship by means of simulations. Verwilligen et al. (2022) studied the accessibility of the Ghent-Terneuzen canal for the widest allowed ship, in a very restricted and irregular area.

Model tests have been and remain a favoured way to study this complex physical interaction. However, they require significant resources, especially when investigating a large range of ship types and bank geometries. The progress of Computational Fluid Dynamics (CFD) capabilities and its affordability has made numerical predictions a promising complement to model-scale experiments. To build up confidence in the numerical set-ups for such applications and learn more about the underlying physics, it is crucial to benchmark the performance of CFD techniques. This was done for example in Van Hoydonck et al. (2019), which compares a large range of prediction methods to experiments for the KRISO Very Large Crude Carrier (KVLCC2). This need for benchmarking is particularly critical for applications on inland waterways, as they are facing tremendous challenges with the higher seasonal variations of water level and widths of sailable corridors.

This paper compares experimental and numerical results of a test case considering a reference inland waterway vessel sailing along a vertical bank. It documents the experimental and numerical set-ups, and shows ship-bank interaction forces applied to the ship for various water depths and distances to the bank. It also presents a detailed analysis of the predicted flow fields, to understand better the underlying physics and the challenges for prediction techniques in extreme conditions. Finally, the study investigates potential scale effects for such application.

2 TEST CASE

The ship investigated in this study is a representative 135m inland ship of CEMT-class Vb, typically travelling on the river Rhine. This benchmark ship was designed in 2014 by the Federal Waterways Engineering and Research Institute (BAW) and the Development Centre for Ship Technology and Transport Systems (DST). This public hull is the test case of experimental studies focusing on the resistance, propulsion and manoeuvring performance of inland ships in shallow water (Mucha et al., 2017, 2018, 2019). More recently, this reference ship was selected in the SHINING workshop to investigate CFD techniques to predict manoeuvring forces and moments in shallow water (Chilcee et al., 2025).

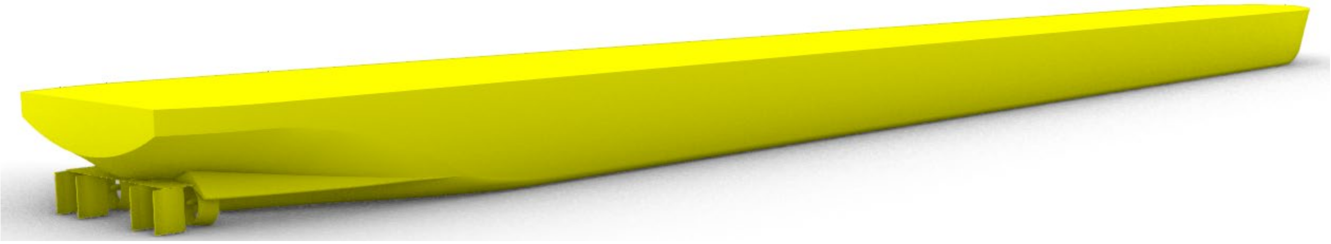

Figure 1. Isometric view of the ship geometry.

Figure 1 shows the ship geometry. The main particulars of the inland waterway ship and its appendages are detailed in Table 1. Characteristics are given for the full scale and at a linear scale ratio of λ = 1:16, since the investigation was mostly conducted at model scale. The ship is equipped with a conventional twin-shaft arrangement with two ducted propellers and four fishtail-type rudders with an endplate. The propellers have a diameter 1.6 m and rotate inward over the top. The duct geometry is similar to the 19A type, but is trimmed horizontally at the bottom at the height of the baseline. The projected lateral area of the rudders is about 4 x 2.36 m^2, which corresponds to 4 x 0.50%·L_{PP}·T. Mucha et al. (2017) provide further information about the aft-ship arrangement.

This study compares numerical and experimental methods to determine ship-bank interactions for the reference ship in shallow water. To ensure a fair comparison, both methods aim at using the same set-up. The ship sails along a regular bank that consists of a vertical wall located on the port side of the ship. A parallel vertical wall is located on the starboard side, further away from the ship. The distance between the two side walls is about 22.1 times the ship width, mimicking a waterway with straight vertical walls. The ship is towed in a semi-captive condition where the surge, sway, roll and yaw motions are imposed, while the heave and pitch are free. This ensures a more realistic equilibrium of forces, as the squat may be large in shallow and confined water and has a strong sensitivity to the hydrodynamic loads, even at low speeds.

Table 1. Main particulars of the inland waterway ship and its appendages.

Designation	Symbol	Full scale	Model scale
Linear scale ratio (-)	λ	1	16
Length between perpendiculars (m)	L_{PP}	135.0	8.438
Breadth moulded on waterline (m)	B	11.44	0.715
Draught at rest, even keel (m)	T	3.50	0.219
Displacement volume (m^3)	∇	4,991.5	1.219
Propeller diameter (m)	D	1.6	0.100
Pitch ratio at 70% radius (-)	P/D	1.000	1.000
Expanded blade area ratio (-)	A_E/A_0	0.679	0.679
Number of blades (-)	Z	4	4
Rudder height (m)	b	1.726	0.108
Rudder chord (m)	c	1.370	0.086

The ship is sailing straight at a constant speed V_s with zero drift and roll. The investigation includes various distances between the portside bank and the closest ship side *d*, and various water depths *h*. They are expressed in a non-dimensional way, as a ratio of the ship breadth (*d/B*) and ship draught at rest (*h/T*). The propellers are rotating at a fixed revolution rate (*RPM*), that is close to the model-scale self-propulsion point at the given water depth but in horizontally-unrestricted water. The rudders are fixed to their neutral angle. Table 2 lists the stationary conditions that are presented in this article.

Table 2. Matrix of stationary conditions (quantities are indicated at model scale).

Configuration	h/T (-)	Vs (m/s)	d/B (-)	RPM (1/min)	δ (deg)	F_{rh} (-)	V_s/V_{cr} (-)	EXP (-)	CFD MS (-)	CFD FS (-)
Appended	3.0	0.972	1.5	303	0	0.38	0.45	✓	✓	✓
Appended	1.5	0.972	1.5	322	0	0.54	0.69	✓	✓	✓
Appended	1.2	0.972	1.5	341	0	0.61	0.79	✓	✓	✓
Appended	1.5	0.972	2.5	322	0	0.54	0.69	✓		
Appended	1.5	0.972	2.0	322	0	0.54	0.69	✓	✓	
Appended	1.5	0.972	1.0	322	0	0.54	0.69	✓	✓	
Appended	1.5	0.972	0.5	322	0	0.54	0.69		✓	

EXP: experiments, CFD MS: CFD calculations at model scale, CFD FS: CFD calculations at full scale

All conditions are performed at the model-scale speed of 0.972 m/s, which corresponds to 14 km/h at full scale and a Froude number of F_r = 0.107. The depth Froude F_{rh} number ranges between 0.38 and 0.61. The cross-section of the waterway results in a horizontal restriction and potential confinement effects. The lowest water depth results in a blockage factor of *S* = 4.5%. The critical canal speed (or Schijf-limiting speed) V_{cr} is the speed that ships cannot exceed due to the energy balance between the continuity equation and Bernoulli's Law (Schijf, 1949). The most extreme condition is performed at a relatively high-speed corresponding to $V_s = 0.79 \cdot V_{cr}$, which is an interesting stress test both for the experimental and numerical set-ups.

3 EXPERIMENTAL AND NUMERICAL SET-UPS

The experimental campaign was held at MARIN in 2024. The model tests were carried out in the Shallow-Water Basin, which measures 220m x 15.8m in length and width. Its bottom is a fixed concrete floor. The water level can be adjusted between 0 and 1.1 m by pumping water in or out.

The testing facility features a towing carriage that travels in the longitudinal direction. The ship model is fixed to the carriage by means of 2 cardan joints. Both cardan joints have a heave and pitch freedom, and the backward joint have an additional surge freedom. In that way, the ship model is free to heave and pitch, but is restricted in all other directions. Each cardan joint is mounted on a force measurement frame, from which the hydrodynamic loads on the ship model are recorded. Figure 3 shows the basin carriage and the test set-up. More information on the basin can be found in Tonelli et al., 2015, including a study on the roughness of the basin bottom and its compliance with the ITTC shallow water guidelines.

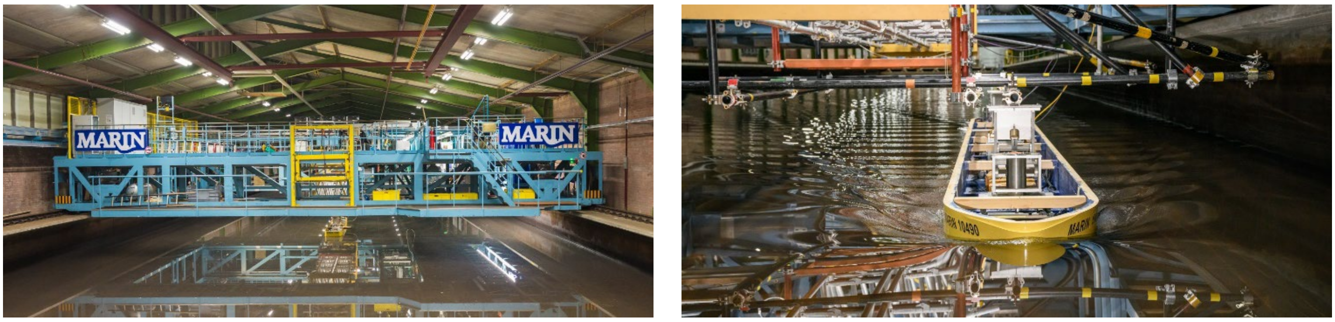

Figure 3. MARIN's Shallow-Water Basin and test set-up.

The calculations are performed with MARIN's CFD package ReFRESCO, which solves multiphase steady and unsteady incompressible viscous flows using the Navier-Stokes equations, complemented with turbulence models. The reliability, robustness and accuracy of the code have been tested for a large range of applications, such as in Bhushan et al. (2019). The ship domain is discretised with unstructured hexahedral elements generated with the commercial software Hexpress. The height of the first cell near the wall *y+* is kept under 0.1 to resolve the boundary layer and guarantee the turbulence model's stability. Table 3 summarises the main particulars of the numerical domain and mesh.

Table 3. Numerical domain and mesh.

Parameter name	Values
Computational domain size (m)	93 x 15.8 x 26
Type of grid (-)	Unstructured, hexahedral
Number of grid cells (-)	30-50 million
Thickness first viscous layer cell (-)	*y+* ~ 0.08

Figure 4 shows a 3D view of the domain as well as some details of the grid at the ship stern. The width of the domain is equivalent to the width of the towing tank where the experiments are conducted. In the calculations, the ship is free to heave and pitch by means of a quasi-static method. The computed squat is modelled through local grid deformation using radial basis functions. All vertical side boundaries are modelled as inflow boundaries with a fixed velocity condition. The top of the domain is implemented as a pressure boundary with homogeneous condition for the pressure. The bottom is modelled as a no-slip wall. The k-ω SST (2003) model from Menter (1994) is used in the URANS turbulence equations. This turbulence model offers good robustness and accuracy for this type of application, and was successfully used in numerous ship hydrodynamic-related CFD computations, such as in Bhushan et al. (2019).

A second-order (limited) scheme is employed for the spatial discretisation of the momentum equations, while the turbulence equations are solved using a first-order upwind discretisation. The linear systems from both of these equations are solved using a GMRES solver with a block Jacobi preconditioner. The pressure system is solved using a preconditioned Conjugate Gradient method (Klaij and Vuik, 2013). The resulting set of equations is solved in a segregated manner. A two-phase flow (water and air) is simulated using the Volume of Fluid (VoF) approach.

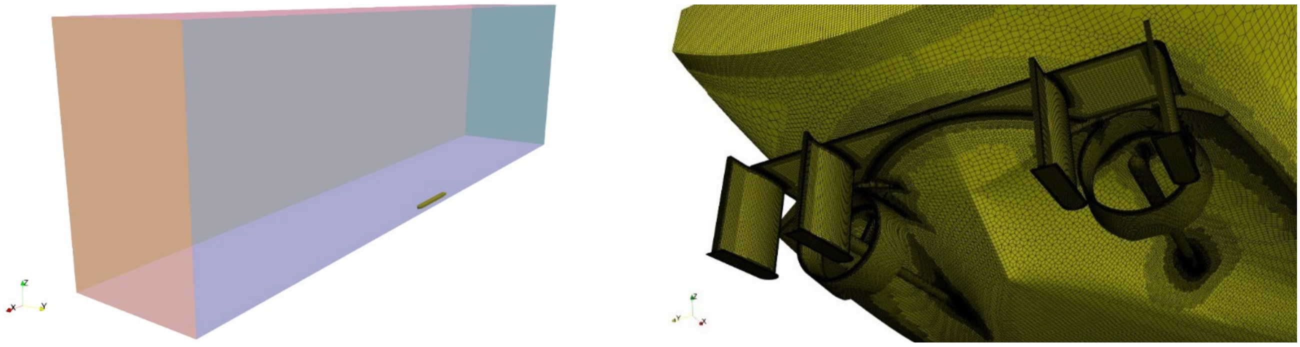

Figure 4. Computational domain (left) and details of the grid at the ship stern (right).

The time-dependent simulations are solved with a first-order (implicit Euler) time integration method. The time step is chosen to 2% of the characteristic time L_{PP}/V_S. The equation governing the free-surface transport uses three sub-cycling steps within each outer-loop iteration.

New ReFRESCO features are verified in these simulations. These improvements include a better correction for grid non-orthogonality, helping to achieve a higher order of discretisation. The grid deformation enabling trim and sinkage, which uses radial-based functions, is also revised to maintain a higher grid quality after deformation. Besides, free-surface sub-cycling is optimised, allowing different time steps to solve momentum and free-surface equations, therefore drastically reducing calculation costs. Finally, the latest version of adaptive grid refinement is implemented to increase grid density in the relevant regions, such as vortices or flow separations.

4 RESULTS AND DISCUSSION

This section presents and discusses the main findings of the study. It is divided into three aspects: the effect of the under-keel clearance, the effect of the distance to the bank, and the scale effects. To refer to the different configurations, figures use the following labels:

- **EXP**: experimental results.
- **CFD MS**: CFD calculations at model scale.
- **CFD FS**: CFD calculations at full scale.

Ship forces and moments are expressed in a ship-fixed coordinate system R_0. The origin is located at the intersection between the midship section (station 10), the centreline, and the waterline at rest. The x-, y-, and z-axes point forward, to portside, and upward respectively.

The ship sway force and yaw moment are given in a non-dimensional form, using the ship speed V_s, fresh-water density ρ and draught at rest T. These non-dimensional loads are defined as follows:

$$F_Y' = \frac{F_Y}{0.5\,\rho\,L_{PP}\,T\,V_S{}^2} \qquad M_Z' = \frac{M_Z}{0.5\,\rho\,L_{PP}{}^2\,T\,V_S{}^2} \tag{1}$$

With F_Y and M_Z the sway force and yaw moment respectively. The effect of confinement on the surge force has been studied in detail in numerous earlier publications, therefore it is not the point of attention of this paper. The dynamic sinkage z' is expressed as a ratio of the ship draught:

$$z' = -\frac{z}{T} \tag{2}$$

4.1 EFFECT OF UNDER-KEEL CLEARANCE

This section presents the results at an intermediate distance to bank of d/B = 1.5 for various water depths. Figure 5 shows the sway force and yaw moment acting on the ship at water depth-to-draught ratios of h/T = 3.0, 1.5, and 1.2. In all conditions, the ship experiences a transversal suction force (positive F_Y') towards the vertical bank. The centre of application of this force is located aft of midship, as illustrated by the bow-out yaw moment (negative M_Z'). The intensity of the bank effect increases as the under-keel clearance decreases. These first observations are consistent with the experience of shippers and other research studies on bank effects (Lataire et al., 2009, Delefortrie et al., 2024).

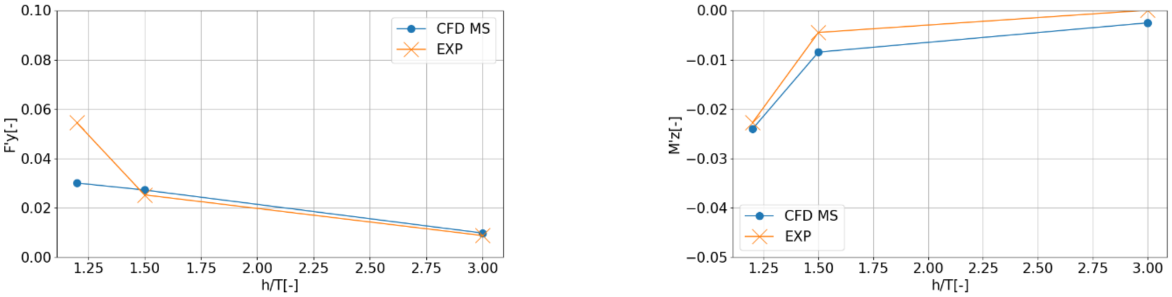

Figure 5. Ship sway force and yaw moment at various water depths (*d/B* = 1.5, F_r = 0.107).

The model tests and numerical predictions show a good qualitative agreement, with the exception of the transverse force in the shallowest condition (*h/T* = 1.2). In this case, the CFD calculation predicts a similar F_Y' compared to a slightly deeper case (*h/T* = 1.5), while the experiments show an increase of more than 100% between these two under-keel. The complexity of predicting accurately the transverse component of the bank suction in such extreme shallow water was also identified in previous investigations, such as a comprehensive study considering the sea-going crude carrier KVLCC2 (Van Hoydonck et al., 2019). The source of the discrepancy is not entirely known. However, the experimental F_Y' results in the shallowest condition were very sensitive to propeller rotation rate. In the cases with the water-milling propeller, no sudden increase in the F_Y' was found. This indicates that an accurate modelling of the flow around the propellers in the shallowest case is critical. In the CFD calculations, the propellers were simulated using the actuator disk model, which could be too simple to mimic the behaviour of the propellers in cases with the smallest under-keel clearance. Indeed, at low under-keel clearance the propeller inflow velocity reduces due to the hull blockage effect, characterised by an increase in wake fraction. In severe conditions, flow separation in front of the propeller can even occur. The increase in propeller loading substantially affects the dynamic pressure and hydrodynamic force distributions, but is not captured by the actuator disc model.

Figure 6 presents the results of the squat. The dynamic sinkage increases as the under-keel clearance decreases, going from around 0.03 in the deepest case (*h/T* = 3.0) to more than 0.10 in the shallowest condition (*h/T* = 1.2) based on experimental results. The trim angle remains however very small and never exceeds -0.06 deg (stern down).

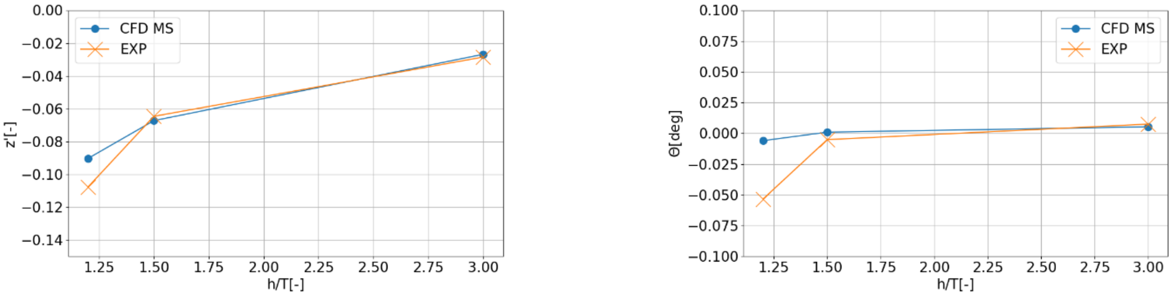

Figure 6. Dynamic trim and sinkage at various water depths (*d/B* = 1.5, F_r = 0.107).

The numerical predictions share the same trends as the model tests and have an excellent agreement up to *h/T* = 1.5. In lowest under-keel clearance, CFD results slightly underpredicts the dynamic sinkage and trim (stern down) compared to the model tests. This may partially explain the underprediction in F_Y' for this condition.

CFD allows to look more in-depth at the underlying physical phenomena, for instance by looking at the force distribution along the hull, the dynamic pressure coefficient on the appended ships and on the waterway bottom and side wall, and the longitudinal velocity fields. Figure 7 presents the distribution of the transverse bank-suction force F_Y' at each station (i.e. a ship cross-section). Integrating this force along the complete hull results in the same total F_Y' indicated in Figure 5. Similarly, integrating this force while multiplying by the distance to midship results in the total yaw moment M_Z'.
The ship bow experiences a repulsion force from the bank between stations 16 and 20, which is slightly behind the fore-shoulder. The transverse force reverses from this point and until the beginning of the tunnel, approximately at station 3. In this range where the ship cross-section is constant, the force is directed towards the bank. The forces vary more in the aft ship, but a small suction force can be observed between stations 0 and 1, at the location of the rudders and ducts.

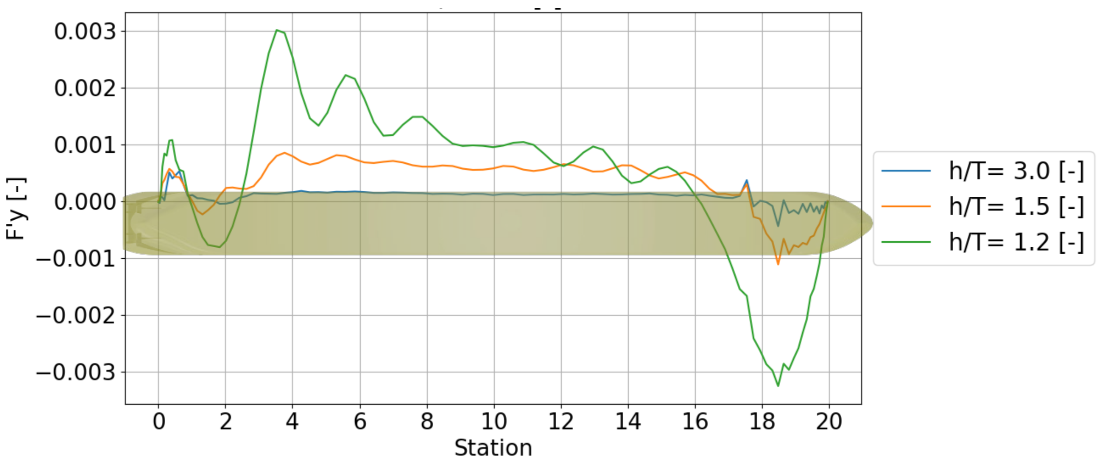

Figure 7. **Distribution of sway force along the hull at various water depths (*d/B* = 1.5, F_r = 0.107).**

The under-keel clearance has a very strong effect on the intensity of the local transverse force. The integrated repulsion force at the bow varies with more than a factor 5 between *h/T* = 1.5 and *h/T* = 1.2. The suction force along the midship cross-section increases also to the same extent. However, the total F_Y' predicted by the CFD calculations has the same intensity, as pointed out in Figure 5. This evidences that the transverse bank force is a force of low intensity, resulting from the difference between two large forces of opposite directions. Therefore, a minor prediction error of either of these forces will result in a large error of the total bank suction force. This may partly explain the challenges to reliably and accurately predict such force with numerical methods for extreme shallow-water conditions such as *h/T* = 1.2. On the other hand, both these forces result in yaw moments of the same sign. Therefore, the numerical prediction of the yaw moment may then be less sensitive to the CFD modelling.

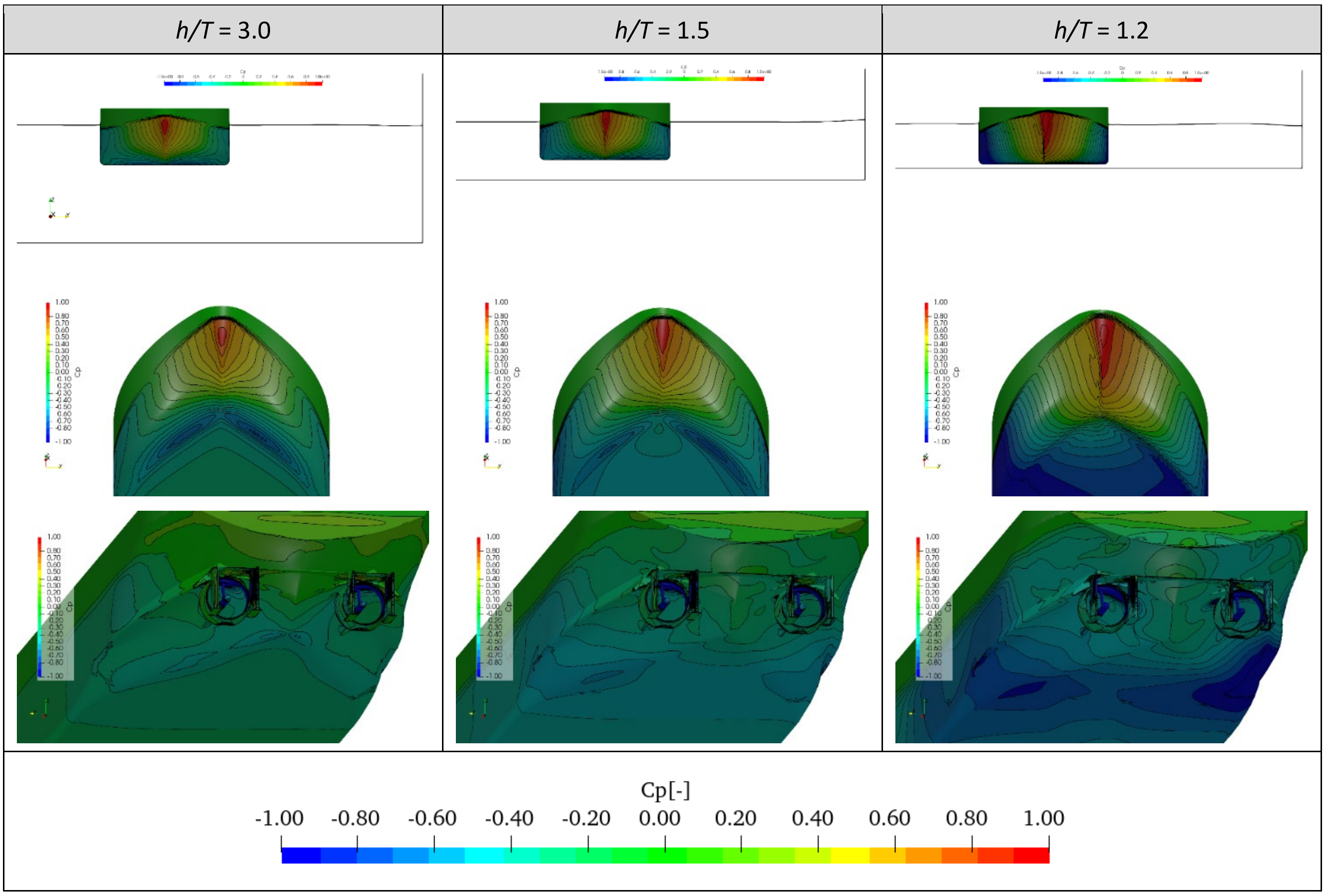

Figure 8. **Dynamic pressure coefficient on the appended ship at various water depths (*d/B* = 1.5, F_r = 0.107).**

Figure 8 plots the dynamic pressure coefficient on the bow and stern of the appended ship. The same high-pressure and low-pressure regions can be observed at all water depths, but with an increasing intensity as the under-keel clearance decreases. At *h/T* = 1.2, the strong low-pressure area on the ship bottom illustrates the accelerated flow travelling under the ship keel and explains the increased squat. At the same time, the asymmetry in the pressure field becomes more marked between the portside and starboard side of the hull, in particular at the bow.

Similarly, Figure 9 shows the dynamic pressure coefficient on the waterway bottom and bank surrounding the ship. It can be seen that the zone of influence of the ship grows in shallower water, both in the longitudinal and transverse directions. At *h/T* = 1.5 and lower, this zone extends to the opposite bank of the waterway. This emphasizes the confinement effect on the ship, which then interacts with both vertical walls.

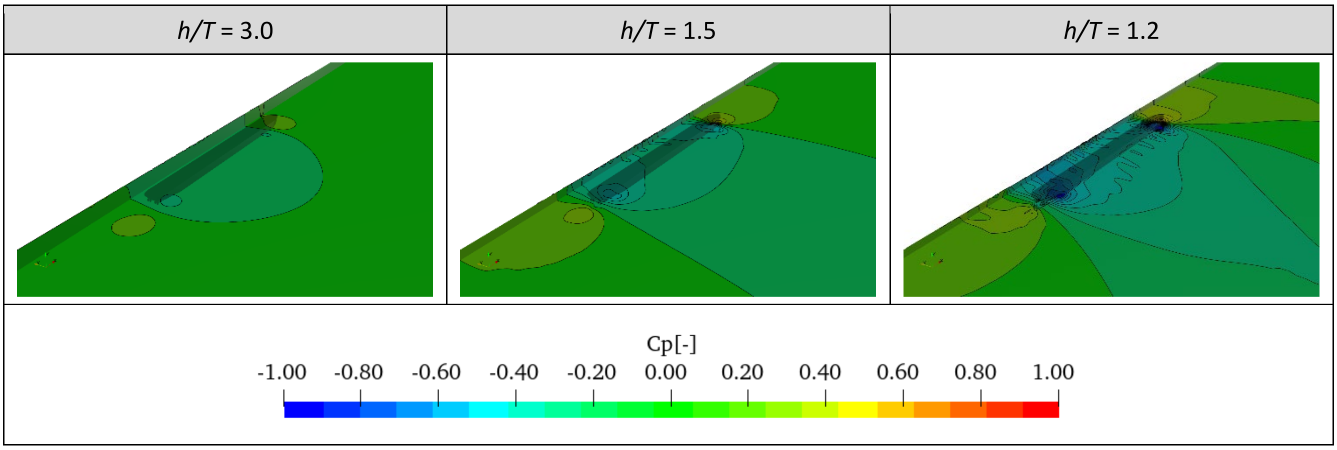

Figure 9. **Dynamic pressure coefficient on waterway bottom and side wall at various water depths (*d/B* = 1.5, F_r = 0.107).**

Figure 10 displays the flow longitudinal velocity between the ship and the bank for cross-sections located at ship stations 0, 10 and 17. The blue colour in the flow field indicates where the water is still. The red colour shows the regions where the flow velocity is opposite to the direction of the ship, evidencing a return flow. The purple colour represents the boundary layer, indicating the regions where the flow travels in the same direction as the ship.

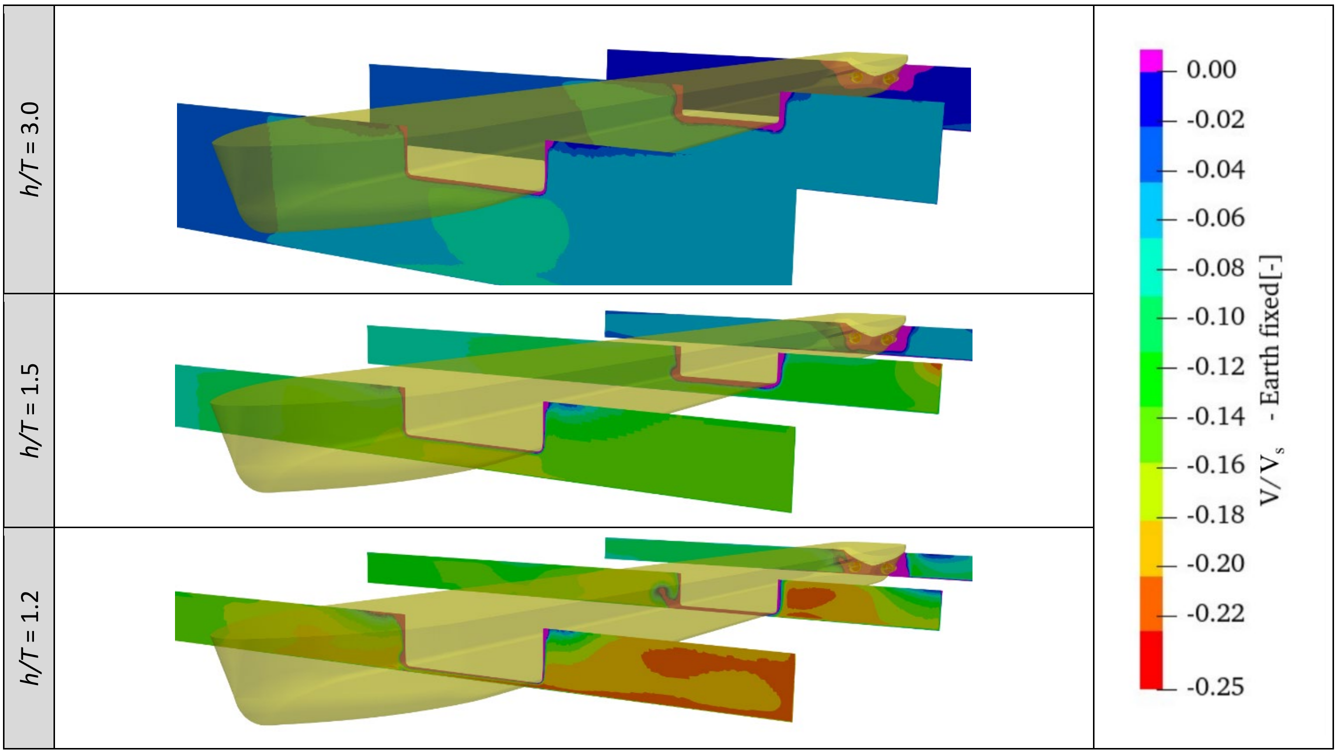

Figure 10. **Longitudinal velocity fields at stations 0, 10 and 17 between the ship and vertical bank at various water depths (*d/B* = 1.5, F_r = 0.107).**

Figure 10 shows that the under-keel clearance strongly influences the intensity of the return flow under the ship, between the ship and the closest bank, but also on the open side (here starboard side). The deep-water case evidences little disturbance of the flow field between the ship and the side wall. The water displaced by the ship travels under the ship, where the return flow is in the range of -0.08V_s. As the water level decreases, less water can travel under the hull. It is instead displaced laterally, and in particular between the hull and the closest wall. In the case *h/T* = 1.2, the magnitude of the return flow velocity is up to 25% of the ship speed in the region near the side wall. It can also be seen that the return flow is more pronounced in the bow than near the stern. The lower cross-section area at the stern and the suction of the propellers contribute to this phenomenon.

As a summary of the previous observations, the results show a high sensitivity of the ship-bank interactions to the under-keel clearance. Even at a distance to the closest bank as far as *d/B* = 1.5 (more than 17 m at full scale), the magnitude of the repulsion force at the bow and the suction force on the rest of the ship increase by at least a factor two between *h/T* = 1.5 and *h/T* = 1.2. Sudden variations in water depth may result in unexpected bank effects, demanding immediate correction from the captain to limit the change in trajectory.

4.2 EFFECT OF DISTANCE TO BANK

This section explores the sensitivity of the bank effects to the distance between the ship and the bank, indicated as *d/B*. Figure 11 shows the sway force and yaw moment acting on the ship at a distance to the bank *d/B* between 2.5 and 0.5, for a sailing speed V_s of 0.972 m/s and an intermediate water depth-to-draught ratio of *h/T* = 1.5. This speed and confinement can typically be encountered in rivers and canals, with a blockage factor *S* of 3%, a depth Froude number F_{rh} of 0.54, and a speed corresponding to 76% of the critical canal speed V_{cr}. Nevertheless, the narrowest distance between the ship and the bank is *d/B* = 0.5, which is about 5.7 m at full scale and is considered as an extreme condition.

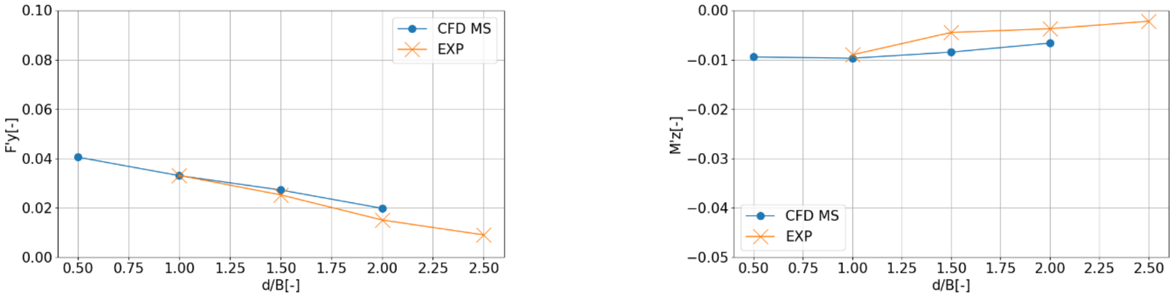

Figure 11. Ship sway force and yaw moment at various distances to the bank (*h/T* = 1.5, F_r = 0.107).

As expected from literature, the ship experiences a transversal suction force (positive F'_Y) towards the vertical bank. The centre of application of this force is located behind midship, as illustrated by the bow-out yaw moment (negative M'_Z). The intensity of the bank effect increases as the distance to the bank reduces. The results show a roughly linear trend for this range of *d/B* and more modest compared to the trend observed with respect to the water depth. Figure 12 shows that the squat is only mildly impacted by the distance to the bank, with only minor differences between *d/B* = 2.5 and 0.5. Experiments and numerical predictions show comparable trends.

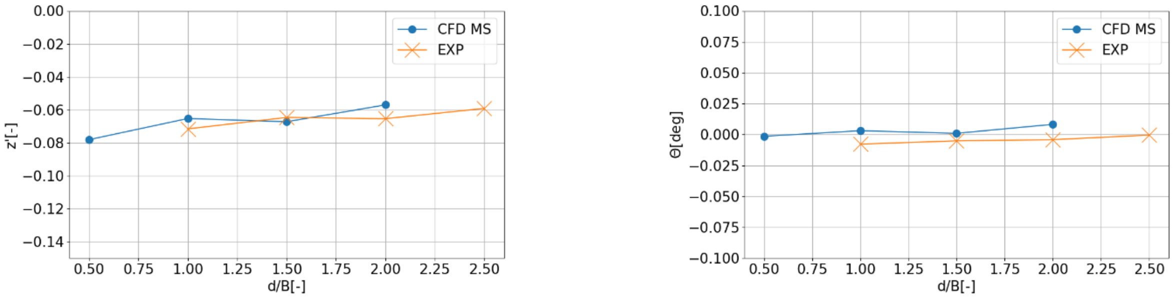

Figure 12. Dynamic trim and sinkage at various distances to the bank (*h/T* = 1.5, F_r = 0.107).

Figure 13 presents the distribution of the transverse bank-suction force F'_Y at each station. All distances to bank show a magnitude of the repulsion force at the bow of a comparable order, slightly increasing as the ship gets closer to the bank. A similar observation can be made about the suction force spread over the midship cross-section.

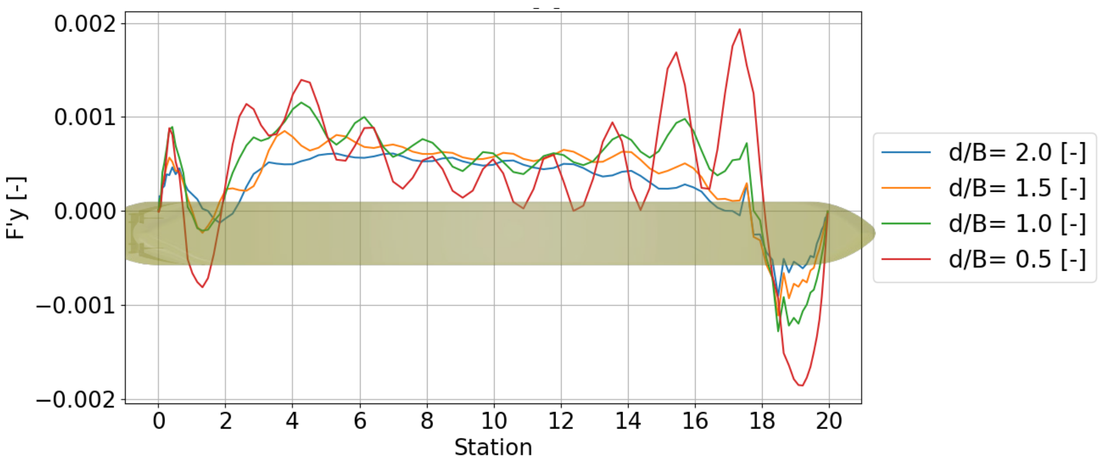

Figure 13. **Distribution of sway force along the hull at various distances to the bank (*h/T* = 1.5, F_r = 0.107).**

This can also be seen in Figure 14, which displays the dynamic pressure coefficient on the bow and stern of the appended ship. The pressure gradients are qualitatively similar at all distances to bank, with slightly more pronounced asymmetry at *d/B* = 0.5. This can be seen in the low-pressure peak on the port side of the ship bottom near the fore shoulder.

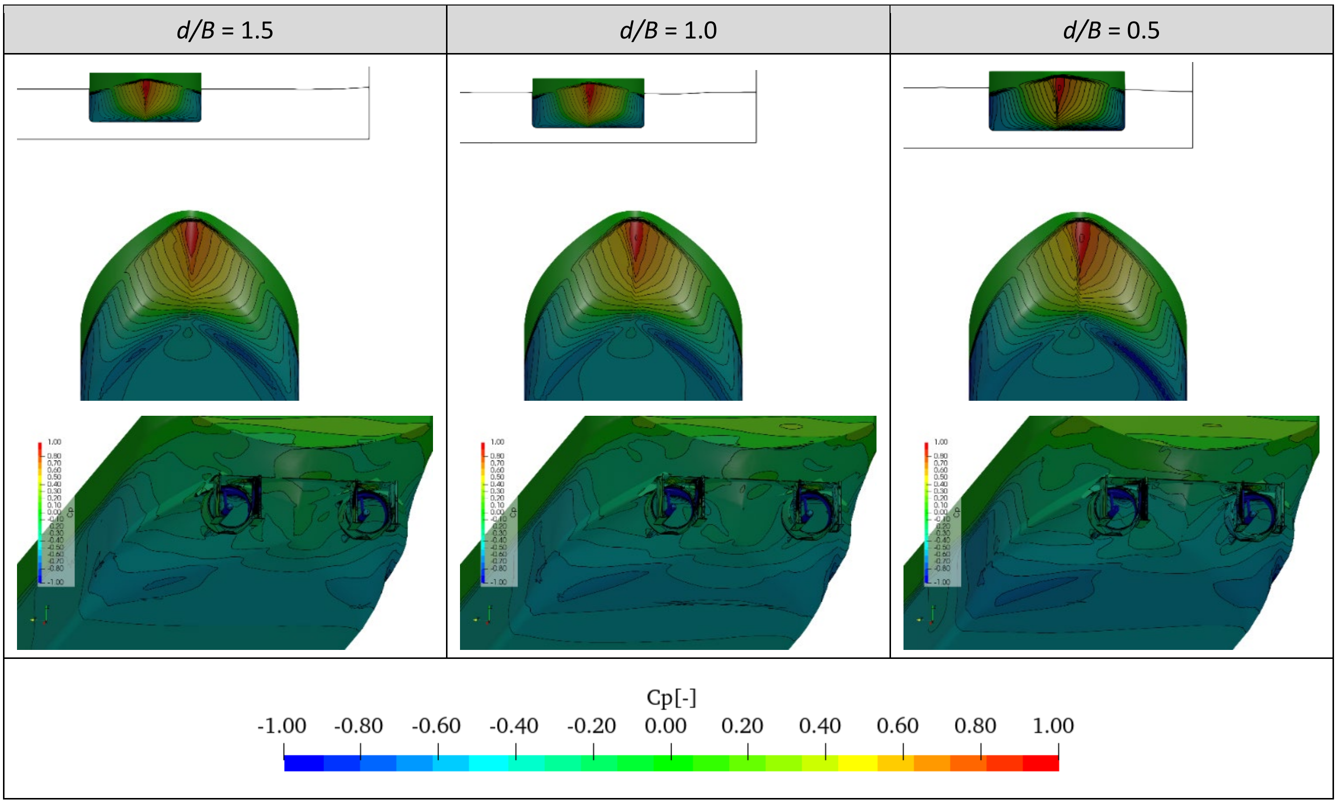

Figure 14. **Dynamic pressure coefficient on the appended ship at various distances to the bank (*h/T* = 1.5, F_r = 0.107).**

Figure 15 shows the dynamic pressure coefficient on the waterway bottom and bank surrounding the ship. It can be seen that the zone of influence of the ship is similar for all three cases, since they all correspond to the same blockage coefficient. Nevertheless, the intensity of the pressure on the wall is greater when the ship is closer, as expected. This illustrates the risks of degradation of natural banks, which are under more stress when ships sail too close.

Figure 16 displays the flow longitudinal velocity between the ship and the bank for cross-sections located at ship stations 0, 10 and 17. The variation in *d/B* shows similar trends as the variation in *h/T* on the velocity field near the ship. The return flow speed between the ship and the bank, in particular at the bow (station 17), is particularly sensitive to *d/B*. At this water depth, only a limited amount of water can flow under the keel and must therefore travel to the sides. When the area between the ship and the bank is too small, for example in the case *d/B* = 0.5, the return flow near the bank is sucked under the hull, not only moving backwards but also from portside to starboard. This can be seen by the eddy on the starboard side of the hull on station 10 slice.

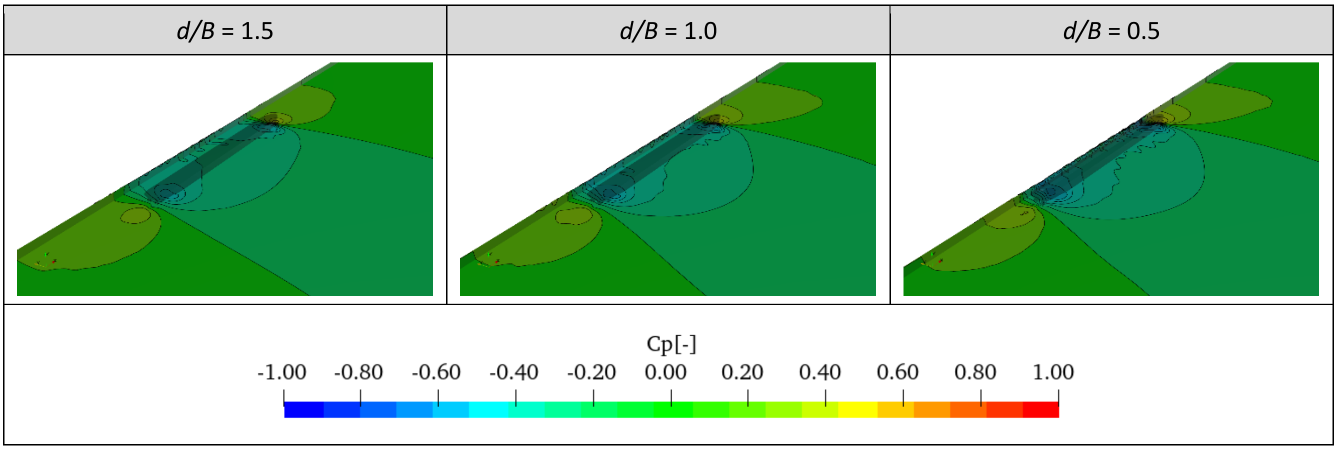

Figure 15. Dynamic pressure coefficient on waterway bottom and side wall at various distances to the bank (h/T = 1.5, F_r = 0.107).

As a summary, the test case illustrates the sensitivity of the ship-bank interactions to the distance between the ship and the bank. The hydrodynamic loads seem to increase linearly as the ship is closer to the bank, but keeping the same order of magnitude for the range of distances investigated in this study. Experiments and numerical predictions show comparable results.

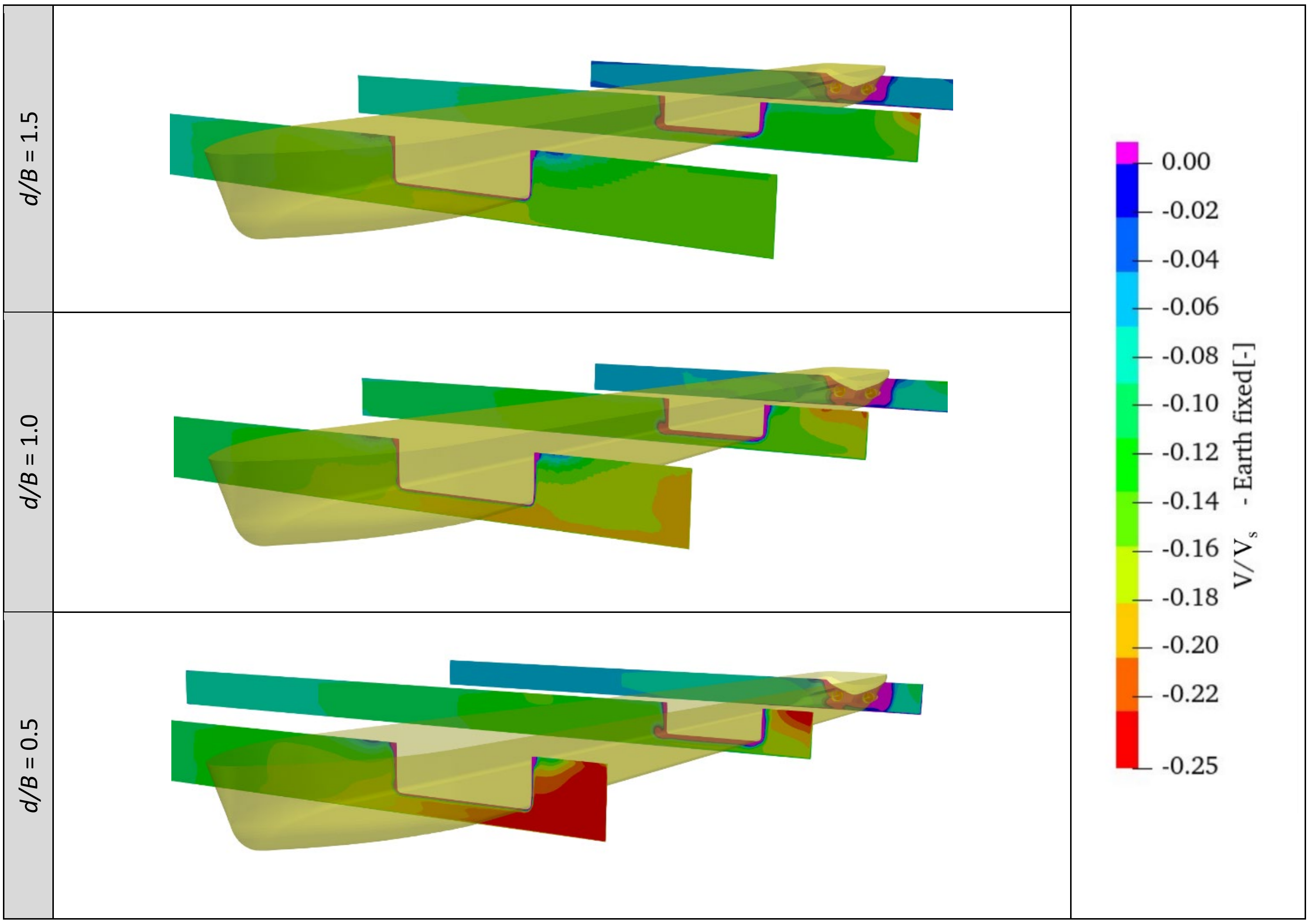

Figure 16. Longitudinal velocity fields at stations 3, 10 and 17 between the ship and vertical bank at various distances to the bank (h/T = 1.5, F_r = 0.107).

4.3 SCALE EFFECTS

To investigate scale effects related to bank effects, additional full-scale CFD calculations were carried out and are presented in this section. Figure 17 shows the sway force and yaw moment acting on the ship at a distance to the bank *d/B* of 1.5 and water depth-to-draught ratios *h/T* of 3.0, 1.5, and 1.2. The most tangible difference between model-scale and full-scale predictions is observed in the shallowest case. However, this is known to be a challenging condition resulting from the difference between two large forces of opposite directions, as observed earlier.

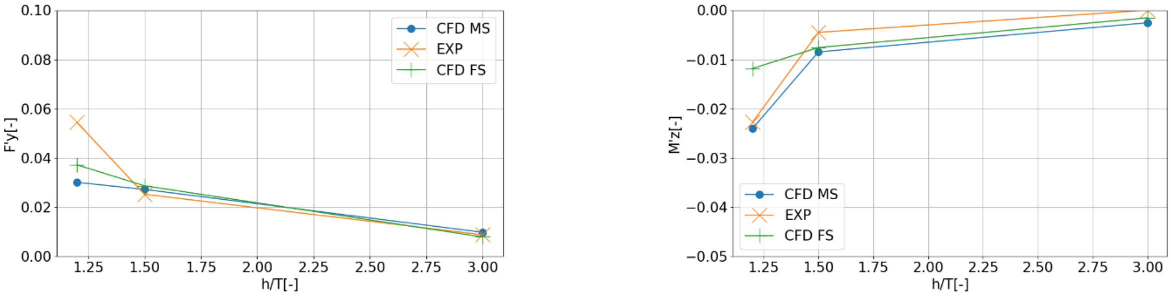

Figure 17. Ship sway force and yaw moment at various water depths, model and full scale (*d/B* = 1.5, F_r = 0.107).

Figure 18 displays the dynamic pressure coefficient at the stern of the appended ship. The pressure gradients are qualitatively the same, with some more marked differences in the shallowest condition.

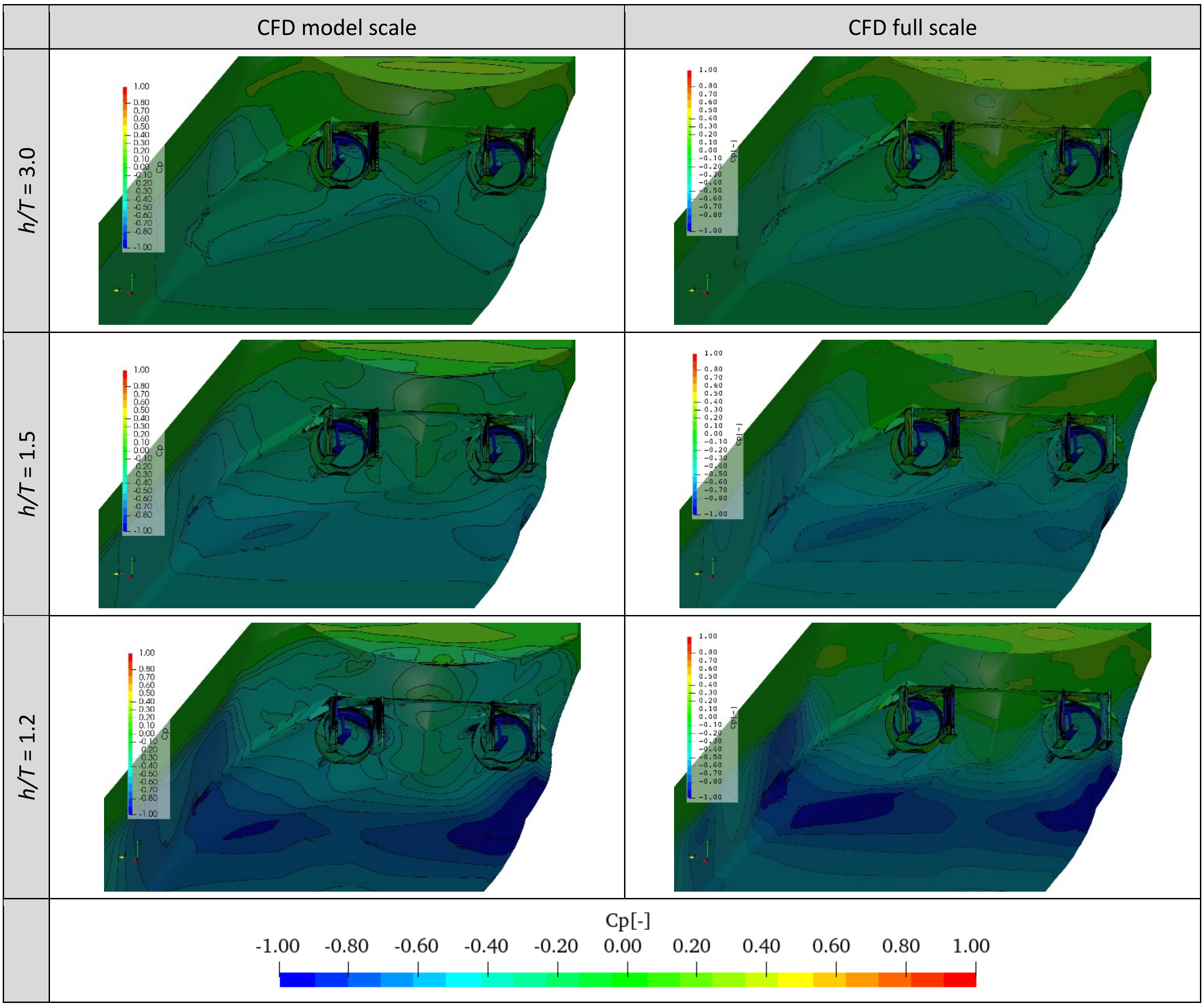

Figure 18. Dynamic pressure coefficient on ship stern at various water depths, model and full scale (*d/B* = 1.5, F_r = 0.107).

Figure 19 displays the flow longitudinal velocity between the ship and the bank for the cross-section located at ship station 10. Here more qualitatively differences are visible. As expected, the boundary layer is larger at model scale. The pattern of the flow fields is quite close between model and full scale, but with some increasing differences in magnitude as the water depth decreases. The return flow speed between model and full scale is basically the same at *h/T* = 3.0. At *h/T* = 1.5, the full-scale CFD calculation predicts more return flow close to the bank. At *h/T* = 1.2, the largest differences between model and full scale are observed close to the ship, with a return flow speed exceeding 25% at model, and only up to 20% at full scale. One of the reasons may be the difference in boundary layer thickness. Since less water is able to travel under the ship in the full-scale computation, due to a thicker boundary layer, the return flow can almost only be on the sides of the ship.

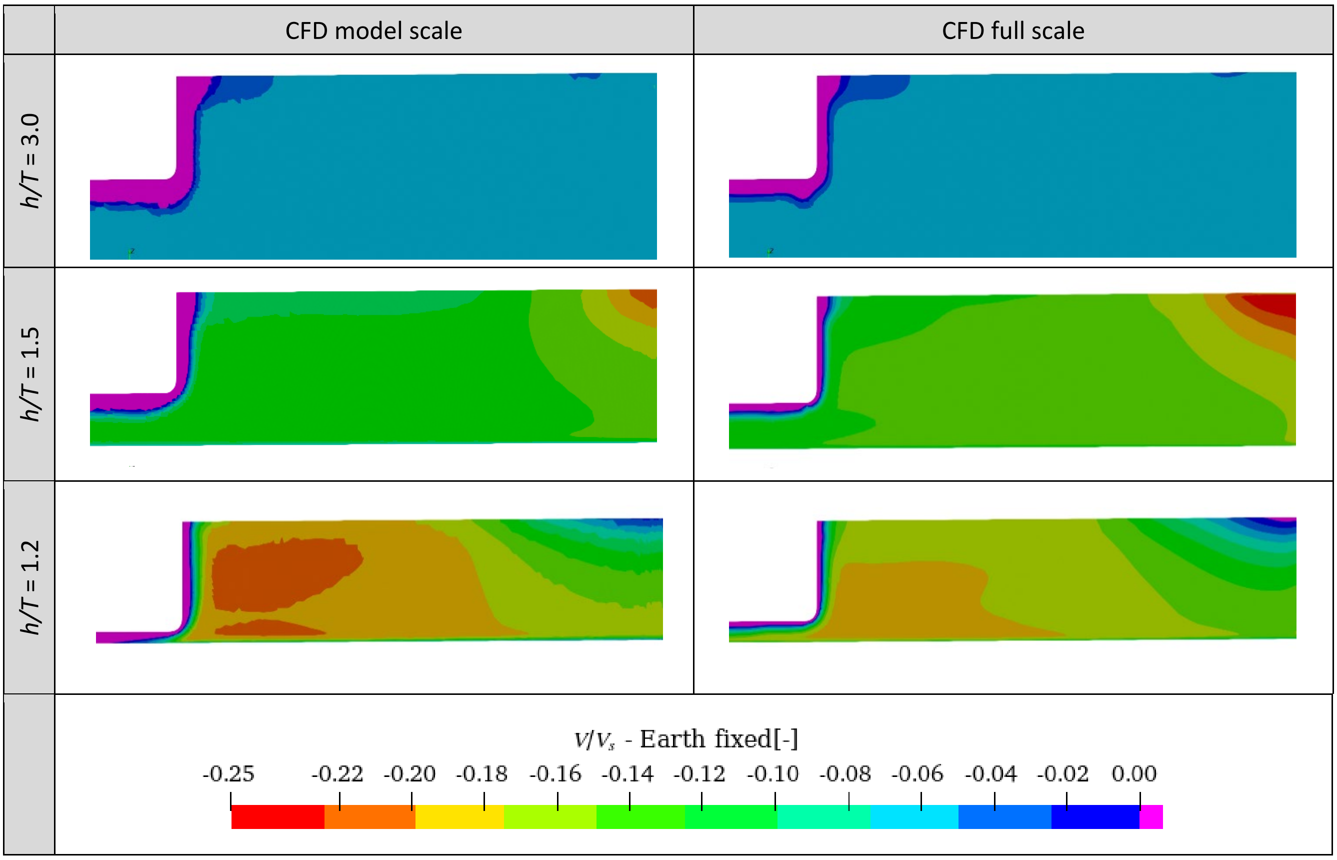

Figure 19. Longitudinal velocity fields at station 10 between the ship and vertical bank at various water depths, model and full scale (*d/B* = 1.5, F_r = 0.107).

This difference is also clearly visible in the force distribution as depicted in Figure 20, showing how larger the force is at model scale. This is particularly noticeable at the bow and around station 3.

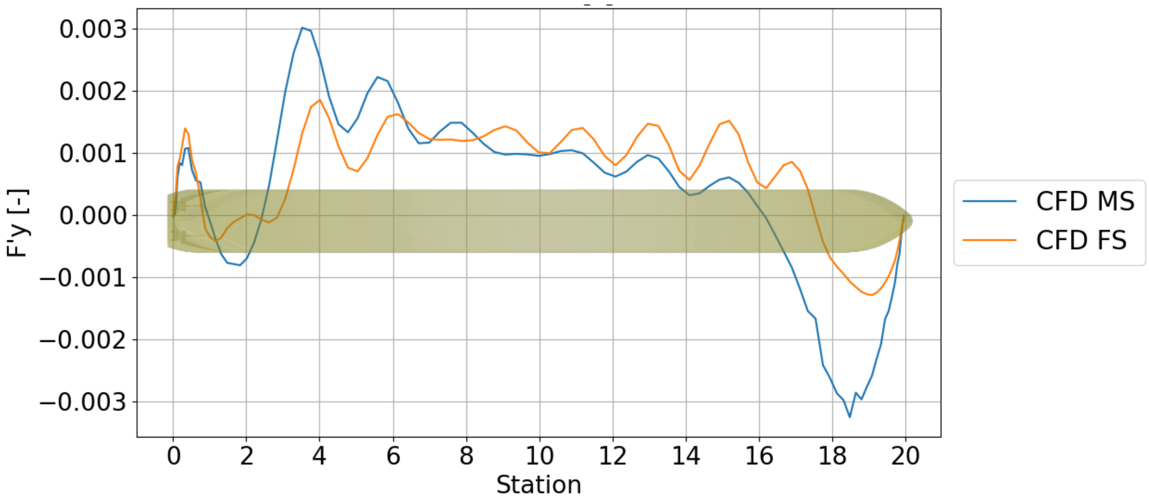

Figure 20. Distribution of sway force along the hull (*h/T* = 1.2, *d/B* = 1.5, F_r = 0.107).

As a summary, the test case illustrates the sensitivity of the ship-bank interactions to the scale effects. Up to *h/T* = 1.5, the hydrodynamic loads seem to be marginally affected by the scale. Discrepancies become larger at a water depth-to-draught ratio *h/T* of 1.2.

5 CONCLUSIONS

This paper presents experimental and numerical methods to identify the bank effects experienced by a representative 135m inland waterway ship sailing along a vertical bank. It compares the total loads acting on the ship as well as the squat, as a function of distances to the bank and under-keel clearances, ranging from 300% to 20%. The numerical predictions share the same trends as the model tests and are consistent with the experience of shippers and other research studies on bank effects. The two methods show an excellent agreement up to medium shallow water (*h/T* = 1.5). In the lowest under-keel clearance (*h/T* = 1.2), CFD results deviate from the experiments by underpredicting the transversal force and the squat motions.

CFD allows a deeper analysis of the underlying physical phenomena by looking at force distributions, but also pressure and velocity fields. The force distribution along the hull evidences that the transverse bank force is a force of low intensity, but resulting from the difference between two large forces of opposite directions. This may partly explain the challenges to reliably and accurately predict such force with numerical methods for extreme shallow water conditions (*h/T* = 1.2). Pressure distributions on the bank also illustrate also the risks of degradation of natural banks when ships are sailing too close.

The paper demonstrates the high sensitivity of ship-bank interactions to the under-keel clearance. Even at a distance to the closest bank as far as *d/B* = 1.5 (more than 17 m at full scale), the magnitude of the repulsion force at the bow and the suction force on the rest of the ship increase by at least a factor two between *h/T* = 1.5 and 1.2. Sudden variations in water depth may result in unexpected bank effects, even for vertical banks. This would require immediate correction from the captain to limit the change in trajectory. This underlines the importance of monitoring the bathymetry of rivers and accurately modelling bank effects in navigation simulators for training and research purposes.

Scale effects, such as a thicker boundary layer at model scale, were also identified. Results show that up to medium-shallow water depth (*h/T* = 1.5), the hydrodynamic loads seem to be marginally affected by the scale. Discrepancies become larger at a water depth-to-draught ratio *h/T* of 1.2.

Numerical predictions and experiments provide complementary insights on ship-bank interactions. Together, they provide reliable validation material for simulator models, but also a detailed outlook of the underlying physical phenomena.

6 REFERENCES

Bedos, A., Oud, G., De Boer, W., 2019. Impact of an Irregular Bank on the Sailed Trajectory of an Inland Ship. In: Proceedings of the Smart Rivers 2019 Conference. Lyon, France.

Bhushan, S., Yoon, H., Stern F., Guilmineau, E., Visonneau, M., Toxopeus, S.L., Simonsen, C., Aram, S., Kim, S.E., Grigoropoulos, G., 2019. Assessment of Computational Fluid Dynamic for Surface Combatant 5415 at Straight Ahead and Static drift 20 deg. Journal of Fluids Engineering. https://doi.org/10.1115/1.4041229.

Chillcce, G., Zentari, L., Van Hoydonck, W., Bedos, A., Ley, J., Gornicz, T., Yang, Y., Oud, G., Tenzer, M., Rzeszutko, J., el Moctar, O., 2025. Numerical Calculation of Hydrodynamic Forces on Inland Waterway Vessels During Circular Motion in Shallow and Extreme Shallow Waters. Ocean Engineering. Vol. 318. https://doi.org/10.1016/j.oceaneng.2024.120095.

Delefortrie, G., Verwilligen, J., Eloot, K., Lataire, E., 2024. Bank Interaction Effects on Ships in 6 DOF. Ocean Engineering. Vol. 310, Part 1. https://doi.org/10.1016/j.oceaneng.2024.118614.

Klaij, C.M., Vuik, C., 2013. Simple-Type Preconditioners for Cell-Centered, Collocated Finite Volume Discretization of Incompressible Reynolds-Averaged Navier–Stokes Equations. International Journal for Numerical Methods in Fluids. Vol. 71, pp. 830-849.

Lataire, E., Vantorre, M., Eloot, K., 2009. Systematic Model Tests on Ship – Bank Interaction Effects. In: Proceedings of the 1st International Conference on Ship Manoeuvring in Shallow and Confined Water: Bank Effects (MASHCON). Antwerp, Belgium, pp. 9-22.

Lataire, E., Vantorre, M., Delefortrie, G., 2015. Longitudinally Directed Bank Effects. In: Proceedings of the International Conference on Ship Manoeuvrability and Maritime Simulation (MARSIM). Newcastle, UK, pp. 1-14.

Mai, T.L., Jeon, M., Vo, A.K., Yoon, H.K., 2023. A Numerical Study on the Ship–Bank Interaction at Various Water Depths of a Surface Ship. Science Progress. Vol. 106(1). https://doi.org/10.1177/00368504221149624.

Menter, F., 1994. Two-Equation Eddy-Viscosity Turbulence Models for Engineering Applications. AIAA Journal. Vol. 32, pp. 1598-1605. https://doi.org/10.2514/3.12149.

Mucha, P., el Moctar, O., Dettmann, T., Tenzer, M., 2017. Inland Waterway Ship Testcase for Resistance and Propulsion Prediction in Shallow Water. Ship Technology Research. Vol. 64 (2), pp.106-113. https://doi.org/10.1080/09377255.2017.1349723.

Mucha, P., el Moctar, O., Dettmann, T., Tenzer, M., 2018. An Experimental Study on the Effect of Confined Water on Resistance and Propulsion of an Inland Waterway Ship. Ocean Engineering. Vol. 167, pp.11-22. https://doi.org/10.1016/j.oceaneng.2018.08.009.

Mucha, P., Dettmann, T., Ferrari, V., el Moctar, O., 2019. Experimental Investigation of Free-Running Ship Manoeuvres Under Extreme Shallow Water Conditions. Applied Ocean Research. Vol. 83, pp.155-162. https://doi.org/10.1016/j.apor.2018.09.008.

Norrbin, N., 1985. Bank Clearance and Optimal Section Shape for Ship Canals. In: Proceedings of the 26th PIANC International Navigation Congress. Brussels, Belgium, pp. 167-178.

Raven, H., 2019. Shallow-Water Effects in Ship Model Testing and at Full Scale. Ocean Engineering. Vol. 189. https://doi.org/10.1016/j.oceaneng.2019.106343.

Schijf, J. B., 1949. Influence on the Form and Dimensions of the Cross-Section of the Canal, of the Form, of the Speed and the Propulsion System of Vessels. In: Proceedings of the 17th PIANC International Navigation Congress, section 1, Inland Navigation. Lisbon, Portugal, pp.61-78.

Tonelli, R., Quadvlieg, F., 2015. New Benchmark Data for Manoeuvring in Shallow Water Based on Free Running Manoeuvring Tests Including Uncertainty of the Results. In Proceedings of the ASME 2015 34th International Conference on Ocean, Offshore and Arctic Engineering. St. John’s, Newfoundland, Canada, Vol. 11. https://doi.org/10.1115/OMAE2015-42254.

Van Hoydonck, W., Toxopeus, S., Eloot, K., Bhawsinka, K., Queutey, P., Visonneau, M., 2019. Bank effects for KVLCC2. Journal of Marine Science and Technology. Vol. 24, pp. 174-199. https://doi.org/10.1007/s00773-018-0545-3.

Verwilligen, J., Lataire, E., Tello Ruiz, M., Eloot, K., 2022. Evaluation of Bank Effects on a Bulk Carrier in a Confined Channel Cased on Towing Tank Tests and Full-Scale Measurement. In: Proceedings of the 6th International Conference on Ship Manoeuvring in Shallow and Confined Water: Port Manoeuvres (MASHCON). Glasgow, UK, pp.285-298.

7 AUTHORS BIOGRAPHY

Antoine Bedos holds the position of Senior Project Manager at the Maritime Research Institute Netherlands (MARIN). He conducts experimental and numerical research for the maritime industry, and has a particular interest for shallow-water and manoeuvring applications. Over the past few years, he has focused on the inland shipping sector. He is also expert in mathematical manoeuvring models and time-domain simulations.

Tomasz Gornicz holds the position of CFD Specialist at the Maritime Research Institute Netherlands (MARIN). He graduated from a technical university in Poland, where his professor, Jan Kulczyk, introduced him to the fascinating world of inland shipping hydrodynamics. For more than 10 years, he has been conducting numerical studies in ship manoeuvring and non-conventional propulsion systems.

Roberto Tonelli holds the position of Senior Researcher at the Maritime Research Institute Netherlands (MARIN). He is also the coordinator of the Manoeuvring research programme within the organisation. He has conducted experimental and numerical research for the maritime industry for more than 10 years. Over the past few years, he has deepened his knowledge and expertise on mathematical manoeuvring models and time-domain simulations.